國立交通大學

應用數學系

碩 士 論 文

有界面活性劑之軸對稱界面在不同黏滯性之流體模擬

Axisymmetric Interfaces with insoluble surfactant in Navier-Stokes flow with different viscosity

研 究 生：楊承翰

指導教授：賴明治　教授

中 華 民 國 九 十 九 年 六 月

有界面活性劑之軸對稱界面在不同黏滯性之流體模擬
Axisymmetric Interfaces with insoluble surfactant in Navier-Stokes flow with different viscosity

研 究 生：楊承翰　　Student：Cheng-Han Yang

指導教授：賴明治　　Advisor：Ming - Chih Lai

國 立 交 通 大 學

應 用 數 學 系

碩 士 論 文

A Thesis

Submitted to Department of Applied Mathematics

College of Science

National Chiao Tung University

in partial Fulfillment of the Requirements

for the Degree of

Master

in

Applied Mathematics

June 2010

Hsinchu, Taiwan, Republic of China

中華民國九十九年六月

有界面活性劑之軸對稱界面在不同黏滯性之流體模擬

學生：楊承翰　　指導教授：賴明治

國立交通大學應用數學學系（研究所）碩士班

摘　　要

本論文把 Immersed boundary method 發展到軸對稱圓柱座標系中來模擬液滴在不可壓縮流中，液滴內外不同的黏滯度是我們所關心的。為方便分佈界面所產生的力至流體以及內插流體流速至界面的移動速度，須藉由 Dirac delta function 將 Eulerian 流體和 Lagrangian 界面變數合併。我們使用 semi-implicit second-order projection method 來解 Navier-Stokes 方程式並且利用 Indicator function 來更新密度和黏滯度。把液滴放入流場中，觀察有加表面活性劑與沒加表面活性劑的差異性。表面活性劑會分佈在界面中，並且影響表面張力的大小。上述的方程式，我們皆加入人工速度去調整界面上網格的位置，使其分佈均勻。

Axisymmetric Interfaces with insoluble surfactant in Navier-Stokes flow with different viscosity

student：Cheng-Han Yang Advisors：Dr. Ming-Chih Lai

Department（Institute）of Applied Mathematics
National Chiao Tung University

ABSTRACT

In this study, the simulation of drop deformation in incompressible flow was executed by developing an immersed boundary method in the axisym metric cylindrical coordinates. The viscosity difference between two sides of drop interface was particularly considered in this paper. We implemented a semi-implicit second-order projection scheme to solve Navier-Stokes equations. Various viscosity between two sides of drop were tested on simulation, as well as the effect of the surfactant on drop, which affect the surface tension. In addition, the distribution of marker positions were stabilized by imposing the artificial velocity and compared to the original manner without imposition of artificial velocity.

誌　　謝

本篇論文的完成，首先要感謝我的指導教授 — 賴明治老師。在老師的細心指點之下，讓我一點一滴熟悉數值偏微分方程以及科學計算的方法。我也從自己的研究中找到對數值偏微分方程以及科學計算這塊領域的興趣與成就感。除了指導教授外，在我們科學計算研究室中的其他學長們也給了我很多的幫助。感謝陳冠羽學長在我剛踏入這塊領域時，指導我撰寫程式語言時所遇到的困難以及課業上的問題。感謝黃仲尹學長與胡偉凡學長很有耐心地教我流體力學的相關理論以及使用 Immersed boundary method 時會碰到的疑難雜症。

在論文口試期間，承蒙吳金典教授與黃聰明教授費心審閱並提供許多寶貴意見，使得本論文變得更加完備，學生永遠銘記在心。

平常除了做數值計算研究外，我也要感謝同一屆的同學們與研究室的學長們，他們與我一起打球，分享彼此的興趣，還有其他好朋友的陪伴如: SFD、GGC 讓我的研究生生活多采多姿，處處充滿著樂趣。

最後，我要好好地感謝我的家人，是他們鼓勵並支持著我做研究的興趣，讓我可以無所顧忌地完成我的學業。希望能與他們，以及在我身邊所有關心我的人，一起分享這篇論文完成的喜悅與榮耀。

目　　錄

1 Introduction

The immersed boundary method was first used in reference to the method developed by Peskin (1972) to simulate cardiac mechanics and associated blood flow. In this paper, we used this method to simulate the behavior of drop in extensional flow using Navier-Stoke equations in cylindrical geometries, where axisymmetric case was performed for convenience of computation. Numerous research has been studied in the subject as above. We attempted to resolve Navier-Stokes equations with various viscosity and density of a drop. Furthermore, we consider the case that surfactant was added on the interface and surfactant, such as soap, detergent, will impact the strength of surface extension.

We first consult [6] and [7] in order to transform the immersed boundary formulation [5] in three-dimensional coordinates into the cylindrical coordinates. Then, we must set the boundary conditions on $r = 0$ such as $u_r = 0$ and $\partial u_z/\partial r = 0$ [6] for our study in the axisymmetric cylindrical coordinates. [5] presented the surfactant concentration equation in Lagrangian coordinates on the interface in the Cartesian coordinates. In order to examine a variety of axisymmetric cases, and according to [10], we should transform the equation into cylindrical coordinates for our study.

Since our initial velocity field has to satisfy Navier-Stokes equations and the axisymmetric boundary conditions, the uniaxial extensional flow $u_r = -0.5rG, u_z = zG$[2] is an optimum. Surfactant on the drifts are flowing along (the direction of) the fluid. Similarly, the flow (has) also affected the markers in Lagrangian coordinates on the interface. The following section will introduce a artificial method about marker redistribution.

The remaining sections of this paper are organized as follows. We present the governing equations in lagrangian coordinates on the interface which includes the immersed boundary formulas and the surfactant concentration equation in section 2. We imposed artificial velocities on some equations to modify the distance between markers. Since viscosity and density are variables in Navier-Stokes equations, we update data of viscosity and density by indicator function. The numerical method which includes an algorithm of solving the Navier-Stokes equations, a mass conservative scheme for the surfactant equation and indicator function is described in section 3. In Section 4, we first examine the convergence of Navier-Stokes equations , then we present the Oscillating drop and observe how much the drop volume leaks or bulks up. we emphasize the effects of the drop deformation on viscosity, surfactant and Peclet number Pe_s, and observe the degree of deformation by [11]. we summarize conclusions and future work in section 5.

2 The governing equations

In this paper, we consider an incompressible two-phase flow problem in a fixed three-dimensional cubic domain.The interface of the drop Σ separates two parts, Ω_1 inside the interface and Ω_2 outside the interface from our domain,which is a simple closed surface immersed in the fluid. i.e.$\Omega = \Omega_1 \bigcup \Omega_2$.

In each fluid region, the Navier-Stokes equations are satisfied as

$$\rho_i \left(\frac{\partial \mathbf{u}_i}{\partial t} + (\mathbf{u}_i \cdot \nabla)\, \mathbf{u}_i \right) = \nabla \cdot \mathbf{T}_i + \rho_i \mathbf{g}, \qquad in\, \Omega_i, \tag{2.1}$$

$$\nabla \cdot \mathbf{u}_i = 0, \qquad in\, \Omega_i, \tag{2.2}$$

$$\mathbf{u} = \mathbf{u}_b, \qquad in\, \partial\Omega, \tag{2.3}$$

where $\mathbf{T}_i = -p_i \mathbf{I} + \mu_i(\nabla \mathbf{u}_i + \nabla \mathbf{u}_i^T)$ is the stress tensor, p_i is the pressure, $\mathbf{u}_i$ is the fluid velocity, ρ_i is the density, μ_i is the viscosity for $i = 1, 2$ in each fluid domain, and $\mathbf{g}$ is the gravitational constant. The velocity is continuous across the interface Σ. Thus,

$$[\mathbf{u}]_\Sigma = \mathbf{u}|_{\Sigma,2} - \mathbf{u}|_{\Sigma,1} = 0 \tag{2.4}$$

and the normal stress jump is balanced by the interfacial force $\mathbf{F}$ (defined only on Σ) as

$$[\mathbf{Tn}]_\Sigma + \mathbf{F} = 0 \tag{2.5}$$

where $\mathbf{n}$ is the unit normal vector on Σ directed towards fluid 2. In this paper, we use the immersed boundary method to approach the velocity solutions of the Navier-Stokes equations. The immersed boundary (the interface) exerts force $\mathbf{F}$ to the fluids and moves with local fluid velocity. For simplicity, gravity is neglected, so the same density of drop is only considered in this study. i.e. $\rho_1 = \rho_2 = \rho$.

To be convenient for calculation, our numerical experiment in the single phase was computed by non-dimensionlizing the following three dimensional equations,

$$\rho \left(\frac{\partial \mathbf{u}}{\partial t} + (\mathbf{u} \cdot \nabla)\, \mathbf{u} \right) = -\nabla p + \nabla \cdot (2\mu E) + \mathbf{f}, \tag{2.6}$$

$$\nabla \cdot \mathbf{u} = 0, \tag{2.7}$$

$$\frac{\partial \Gamma}{\partial t} + (\nabla_s \cdot \mathbf{u})\, \Gamma = D_s \nabla_s^2 \Gamma, \tag{2.8}$$

where $\mathbf{u}$ is the velocity, p is the pressure, ρ is the density, μ is the viscosity, Γ is the surfactant concentration, D_s is diffusivity, and $E = (\nabla \mathbf{u} + \nabla \mathbf{u}^T)/2$ is the rate of deformation tensor.

Assume the dimensionless numbers, $x = r_0 x^*$, $\mathbf{u} = U_\infty \mathbf{u}^*$, $\mu = \mu_0 \mu^*$, $\rho = \rho_0 \rho^*$, $t = (r_0/U_\infty) t^*$, $p = \rho_0 U_\infty^2 p^*$, $\mathbf{f} = f_0 \mathbf{f}^*$, and $\Gamma = \Gamma_\infty \Gamma^*$. Then, the non-dimensional

equations are presented as follows.

$$\rho^* \left(\frac{\partial \mathbf{u}^*}{\partial t^*} + (\mathbf{u}^* \cdot \nabla^*) \mathbf{u}^* \right) = -\nabla^* p^* + \frac{1}{Re} \nabla^* \cdot (2\mu^* E^*) + \frac{r_0 f_0}{\rho_0 U_\infty^2} \mathbf{f}^*, \quad (2.9)$$

$$\nabla^* \cdot \mathbf{u}^* = 0, \quad (2.10)$$

$$\frac{\partial \Gamma^*}{\partial t^*} + (\nabla_s^* \cdot \mathbf{u}^*) \Gamma^* = \frac{1}{Pe_s} \nabla_s^{*2} \Gamma^*, \quad (2.11)$$

where $Re = \rho_0 U_\infty r_0 / \mu_0$ and $Pe_s = r_0 U_\infty / D_s$. In the axisymmetric cylindrical coordinates, we spread the interfacial force into fluid by Dirac delta function $\delta(\mathbf{x}) = \delta(r)\delta(z)$ as follows.

$$\mathbf{f}(\mathbf{x}, t) = \int_\Sigma \mathbf{F}(s, t)\, \delta(\mathbf{x} - \mathbf{X}(s, t))\, ds,$$

where $\mathbf{x} = (r, z)$ is the fluid position, $\mathbf{X}(s, t) = (R(s, t), Z(s, t))$ is the interfacial position, s is the interfacial parameter, $\mathbf{F}$ is the interfacial force, σ is the surface tension, and Σ is the domain of parameter.

Assume the dimensionless number $\sigma = \sigma_0 \sigma^*$, $Ca = \mu_0 U_\infty / \sigma_0$, then we can get

$$\rho^* \left(\frac{\partial \mathbf{u}^*}{\partial t^*} + (\mathbf{u}^* \cdot \nabla^*) \mathbf{u}^* \right) = -\nabla^* p^* + \frac{1}{Re} \nabla^* \cdot (2\mu^* E^*) + \frac{1}{ReCa} \mathbf{f}^* \quad (2.12)$$

$$\nabla^* \cdot \mathbf{u}^* = 0, \quad (2.13)$$

$$\frac{\partial \Gamma^*}{\partial t^*} + (\nabla_s^* \cdot \mathbf{u}^*) \Gamma^* = \frac{1}{Pe_s} \nabla_s^{*2} \Gamma^*. \quad (2.14)$$

The operator forms of governing equaitons in the acisymmetric cylindrical coordintates will be introduced on the following sections. In fact, the characteristic velocity $U_\infty = G r_0$ where G is the principle strain rate and $2r_0$ is the equivalent diameter of the drop. Hence, we have $Re = \rho_0 (G r_0) r_0 / \mu_0$, $Ca = \mu_0 G r_0 / \sigma_0$, and $Pe_s = r_0 U_\infty / D_s$.

2.1 Immersed boundary formulation

In every corner of this paper, we consider the Navier-Stokes equations in cylindrical coordinates instead of Cartesian coordinates,in addition the domain is axisymmetric. Hence, it is convenient to compute our data in a cylindrical coordinate system (r, θ, z). Because of axisymmetric, domain is azimuthal symmetry and the flow depends spatially on only two cylindrical coordinates (r, z). The interface Σ is represented by a parametric form $(r(s,t), z(s,t))$, $0 \le s \le L_b$, where s is the parameter of the initial configuration of the interface, which is not necessarily the arc-length.

The following governing equations can be expressed in the usual immersed boundary formulation using the non-dimenionlization process.

$$\rho\left(\frac{\partial u_r}{\partial t}+u_r\frac{\partial u_r}{\partial r}+u_z\frac{\partial u_r}{\partial z}\right)+\frac{\partial p}{\partial r} = \frac{1}{Re}\left\{\frac{1}{r}\frac{\partial}{\partial r}\left(2\mu r\frac{\partial u_r}{\partial r}\right)+\frac{\partial}{\partial z}\left[\mu\left(\frac{\partial u_r}{\partial z}+\frac{\partial u_z}{\partial r}\right)\right]-\frac{2\mu u_r}{r^2}\right\} + \frac{1}{ReCa}f_r, \tag{2.15}$$

$$\rho\left(\frac{\partial u_z}{\partial t}+u_r\frac{\partial u_z}{\partial r}+u_z\frac{\partial u_z}{\partial z}\right)+\frac{\partial p}{\partial z} = \frac{1}{Re}\left\{\frac{1}{r}\frac{\partial}{\partial r}\left[\mu r\left(\frac{\partial u_r}{\partial z}+\frac{\partial u_z}{\partial r}\right)\right]+\frac{\partial}{\partial z}\left(2\mu\frac{\partial u_z}{\partial z}\right)\right\} + \frac{1}{ReCa}f_z, \tag{2.16}$$

$$\frac{1}{r}\frac{\partial r u_r}{\partial r}+\frac{\partial u_z}{\partial z}=0, \tag{2.17}$$

$$\mathbf{f}(\mathbf{x},t)=\int_\Sigma \mathbf{F}(s,t)\,\delta(\mathbf{x}-\mathbf{X}(s,t))\,ds, \tag{2.18}$$

$$\frac{\partial \mathbf{X}(s,t)}{\partial t}=\mathbf{U}(s,t)=\mathbf{u}(\mathbf{X}(s,t),t)=\int_\Omega \mathbf{u}(\mathbf{x},t)\,\delta(\mathbf{x}-\mathbf{X}(s,t))\,d\mathbf{x}, \tag{2.19}$$

$$\mathbf{F}(s,t)=\frac{\partial}{\partial s}(\sigma(s,t)\boldsymbol{\tau}(s,t))-\frac{1}{R}\frac{\partial Z}{\partial s}(\boldsymbol{\tau}(s,t)\,\mathbf{n}), \tag{2.20}$$

$$\boldsymbol{\tau}(s,t)=\frac{\frac{\partial \mathbf{X}}{\partial s}}{\left|\frac{\partial \mathbf{X}}{\partial s}\right|}=\frac{(R_s,Z_s)}{\sqrt{R_s^2+Z_s^2}}, \tag{2.21}$$

$$\mathbf{n}=\frac{(Z_s,-R_s)}{\sqrt{R_s^2+Z_s^2}}. \tag{2.22}$$

Here, $\mathbf{u}=(u_r,u_z)$ is the velocity of the fluid,(u_r is the radial velocity and u_z is the axial velocity), $\mathbf{U}=(U_r,U_z)$ is the velocity of the drop , σ is the surface tension, $\boldsymbol{\tau}$ is the unit tangent vector on the interface,and $\mathbf{n}$ is the outward normal vector on the interface. The dimensionless numbers are Reynolds number and Capillary number, respectively. The Reynolds number (Re) describing the ratio between the inertial force and the viscous force.The capillary number (Ca) describing the strength of the surface tension. The Eq.(2.17) is the divergence free equation which means continuity. we get the force $\mathbf{f}=(f_r,f_z)$ on the fluid by the Eq.(2.18). Because the Eq.(2.18) represents the interfacial force $\mathbf{F}$ spreads to the fluid, and the force $\mathbf{F}$ on the interface is balanced by the normal stress. The Eq.(2.19) represents the interface was moved by the fluid velocity. The Eulerian ($\mathbf{x}$) and Lagrangian ($\mathbf{X}$) variable are used in the three-dimensional Dirac delta function $\delta(\mathbf{x})=\delta(r)\delta(z)$.The Eq.(2.20) represents the interfacial force $\mathbf{F}$ which arises from the surface tension and its form is derived from Laplace-Young condition.

We consider the case that the drop is contaminated by the surfactant. Let the interface be contaminated by the surfactant, which reduces the surface tension, so that we can find the phenomenon that the surface tension is smaller as the surfactant concentration is higher. The relation between surface tension and surfactant concentration can be described by the linear equation. The following is the approximation of linear equation.

$$\sigma(\Gamma) = \sigma_c(1 - \beta\Gamma), \tag{2.23}$$

where Γ is the surfactant concentration, σ_c is the surface tension of a clean interface, and β is a dimensionless number that measures the sensitivity of surface tension to variation in surfactant concentration.

2.2 Surfactant concentration equation

Since we want to close the system, the surfactant is insoluble to the buck fluids such that it is convected and diffused along the interface. Hence, there is no exchange between the interface and the bulk fluids. Due to those reasons, the total mass of the surfactant must be conserved. The equation of surfactant concentration is derived in this subsection. In the three dimensional cylindrical coordinates, we present a slightly different derivation from Stone [9] for the surfactant transport equation in order to make the total mass of the surfactant conserved.

We can regard the surface as the curve in r-z coordinates in the case of axisymmetric cylindrical coordinates. So, let $L(t)$ be an interfacial segment where the surfactant concentration (the mass of the surfactant per unit surface area) is defined. Since the surfactant on the material element don't transport nor spread to the surrounding (bulk) fluids, the mass on the segment remained consistent.

Hence,

$$\frac{d}{dt}\int_{L(t)} \Gamma(l,t)\, R dl = 0, \tag{2.24}$$

where dl is the arc-length element. In order to apply the time derivative more easily, we rewrite the above equation in terms of the initial parameter s as

$$\frac{d}{dt}\int_{L(0)} \Gamma(s,t) \left|\frac{\partial \mathbf{X}}{\partial s}\right| R ds = 0. \tag{2.25}$$

Further we take the time derivative inside the integral,

$$\int_{L(0)} \left(\frac{\partial \Gamma}{\partial t}\left|\frac{\partial \mathbf{X}}{\partial s}\right| R + \Gamma \frac{\partial}{\partial t}\left(\left|\frac{\partial \mathbf{X}}{\partial s}\right| R\right)\right) ds = 0. \tag{2.26}$$

Note that, the interface and surfactant concentration are tracked in a Lagrangian manner in our present formulation. Thus, the time derivative of the first term in

Eq.(2.26) is exactly the material derivative of Stones derivation. Now we need to compute the rate of the stretching factor, and using Eq.(2.19), we have

$$\begin{aligned}
\frac{\partial}{\partial t}\left(\left|\frac{\partial \mathbf{X}}{\partial s}\right| R\right) &= \frac{\partial R}{\partial t}\left|\frac{\partial \mathbf{X}}{\partial s}\right| + R\frac{\partial}{\partial t}\left|\frac{\partial \mathbf{X}}{\partial s}\right| \\
&= U_r\left|\frac{\partial \mathbf{X}}{\partial s}\right| + R\frac{\frac{\partial R}{\partial s}\frac{\partial}{\partial s}\left(\frac{\partial R}{\partial t}\right) + \frac{\partial Z}{\partial s}\frac{\partial}{\partial s}\left(\frac{\partial Z}{\partial t}\right)}{\left|\frac{\partial \mathbf{X}}{\partial s}\right|} \\
&= U_r\left|\frac{\partial \mathbf{X}}{\partial s}\right| + R\frac{\frac{\partial R}{\partial s}\frac{\partial U_r}{\partial s} + \frac{\partial Z}{\partial s}\frac{\partial U_z}{\partial s}}{\left|\frac{\partial \mathbf{X}}{\partial s}\right|} \\
&= U_r\left|\frac{\partial \mathbf{X}}{\partial s}\right| + R\frac{\frac{\partial R}{\partial s}\left(\nabla U_r \cdot \frac{\partial \mathbf{X}}{\partial s}\right) + \frac{\partial Z}{\partial s}\left(\nabla U_z \cdot \frac{\partial \mathbf{X}}{\partial s}\right)}{\left|\frac{\partial \mathbf{X}}{\partial s}\right|} \\
&= U_r\left|\frac{\partial \mathbf{X}}{\partial s}\right| + \left(\frac{\partial \mathbf{U}}{\partial \boldsymbol{\tau}} \cdot \boldsymbol{\tau}\right) R\left|\frac{\partial \mathbf{X}}{\partial s}\right| \\
&= (\nabla_s \cdot \mathbf{u})\, R\left|\frac{\partial \mathbf{X}}{\partial s}\right|.
\end{aligned} \tag{2.27}$$

Where, the notation $\nabla_s \cdot \mathbf{u}$ means the surface divergence in axisymmetric cylindrical coordinates and $\nabla_s \cdot \mathbf{u} = U_r/R + (\partial \mathbf{U}/\partial \boldsymbol{\tau}) \cdot \boldsymbol{\tau}$. Since the material segment is arbitrary, we can get

$$R\left|\frac{\partial \mathbf{X}}{\partial s}\right|\frac{\partial \Gamma}{\partial t} + R\left|\frac{\partial \mathbf{X}}{\partial s}\right|(\nabla_s \cdot \mathbf{u})\,\Gamma = 0. \tag{2.28}$$

If we permit surfactant diffusion along the interface, we obtain the surfactant transport-diffusion equation as

$$R\left|\frac{\partial \mathbf{X}}{\partial s}\right|\frac{\partial \Gamma}{\partial t} + r\left|\frac{\partial \mathbf{X}}{\partial s}\right|(\bigtriangledown_s \cdot \mathbf{u})\,\Gamma = \frac{1}{Pe_s}\frac{\partial}{\partial s}\left[\left(R\frac{\partial \Gamma}{\partial s}\right) \Big/ \left|\frac{\partial \mathbf{X}}{\partial s}\right|\right] \tag{2.29}$$

where Pe_s (Peclet number) is a dimensionless number relevant in the study of transport phenomena in fluid flows and the boundary condition of Γ is $\partial\Gamma/\partial s = 0$ on $\partial L\,(t)$. We note that surface diffusion is also written in terms of initial parameter s.

2.3 Controlling the interfacial markers uniformly

The interface might be deformed as a velocity field in the domain, which causes our computational markers on the interface to concentrate on some part of interface along the fluid flowing direction. This phenomenon leads into a larger error on the drop volume than the one which interfacial markers are uniformly distributed.

Since drop deformation is only related to the force in the normal direction, we impose an artificial velocity on Eq.(2.19) to redistribute the interfacial markers uniformly. Hence, substitute Eq.(2.19) into

$$\begin{aligned}\frac{\partial \mathbf{X}(s,t)}{\partial t} &= \mathbf{U}(s,t) + U^a(s,t)\boldsymbol{\tau} \\ &= \mathbf{u}(\mathbf{X}(s,t),t) + U^a(s,t)\boldsymbol{\tau} \\ &= \int_\Omega \mathbf{u}(\mathbf{x},t)\,\delta(\mathbf{x}-\mathbf{X}(s,t))\,d\mathbf{x} + U^a(s,t)\boldsymbol{\tau}, \end{aligned} \tag{2.30}$$

where the scalar U^a is the artificial velocity, and it can modify the marker positions such that they avoid being moved by the tangential force. This condition $\partial\left|\partial\mathbf{X}/\partial s\right|/\partial s = 0$ means that the tangential displacement of markers remains unchanged. According to those conditions, we obtain

$$U^a(s,t) - U^a(0,t) = \frac{s}{2\pi}\int_0^{2\pi} \frac{\partial \mathbf{U}}{\partial s'}\cdot\boldsymbol{\tau}' ds' - \int_0^s \frac{\partial \mathbf{U}}{\partial s'}\cdot\boldsymbol{\tau}' ds', \tag{2.31}$$

where $U^a(0,t) = 0$, since we should fix one marker to modify their relative positions.

The new marker positions have changed after adding the artificial velocity term, so Eq.(2.29) has to add some term to preserve that the equation holds. The following is the modified surfactant transport-diffusion equation,

$$R\left|\frac{\partial \mathbf{X}}{\partial s}\right|\frac{\partial \Gamma}{\partial t} + R\left|\frac{\partial \mathbf{X}}{\partial s}\right|(\bigtriangledown_s\cdot\mathbf{u})\,\Gamma - \frac{\partial}{\partial s}(RU^a\Gamma) = \frac{1}{Pe_s}\frac{\partial}{\partial s}\left[\left(R\frac{\partial \Gamma}{\partial s}\right)\Big/\left|\frac{\partial \mathbf{X}}{\partial s}\right|\right]. \tag{2.32}$$

2.4 Density and viscosity equations

Because the drop formation would change as fluid flows by, we have to update the viscosity and density of domain, including inside and outside of the drop, need to be updated using indicator function.

$$I(\mathbf{x},t) = \int_\Omega \delta(\mathbf{x}-\mathbf{X})\,d\mathbf{X},$$

Then, we take gradient to both side to obtain,

$$\begin{aligned}\bigtriangledown I(\mathbf{x},t) &= \bigtriangledown\int_\Omega \delta(\mathbf{x}-\mathbf{X})\,d\mathbf{X}, \\ &= \int_\Omega \bigtriangledown\delta(\mathbf{x}-\mathbf{X})\,d\mathbf{X} \\ , &= -\int_{\partial\Omega}\mathbf{n}\cdot\delta(\mathbf{x}-\mathbf{X})\,ds\end{aligned}$$

Furthermore, we take divergence to both side to obtain,

$$\nabla \cdot \ \nabla I(\mathbf{x},t) = -\nabla \cdot \int_{\partial\Omega} \mathbf{n} \cdot \delta(\mathbf{x}-\mathbf{X})\, ds \tag{2.33}$$

Moreover,

$$\rho(\mathbf{x},t) = \rho_2 + (\rho_1-\rho_2)\ I(\mathbf{x},t), \tag{2.34}$$

$$\mu(\mathbf{x},t) = \mu_2 + (\mu_1-\mu_2)\ I(\mathbf{x},t) \tag{2.35}$$

3 Numerical method

In this paper,computational solution of the fluid flow variables are defined on a staggered grid. This implies that different dependent variables are evaluate at different grid points.

More specifically, the pressure is defined on the grid points labelled as $\mathbf{x} = (r_{i-1/2}, z_{j-1/2}) = ((i-1/2)h, (j-1/2)h)$ for $i = 1,2,\ldots,M, j = 1,2,\ldots,N$, the velocity components u_r and u_z are defined at $(r_{i+1/2}, z_j) = (ih, (j-1/2)h)$,for $i = 1,2,\ldots,M-1, j = 1,2,\ldots,N$ and $(r_i, z_{j+1/2}) = ((i-1/2)h, jh)$,for $i = 1,2,\ldots,M, j = 1,2,\ldots,N-1$,respectively, where the spacing $h = \Delta r = \Delta z$. In addition, the positions of density and viscosity are the same with those of pressure. A accepted staggered grid configuration is shown in Fig.3.1.It can be seen that pressures are defined at the center of each cell while velocity components are defined at the center of the call faces.

For the immersed interface, we use a collection of discrete points $s_k = k\Delta s, k = 1,2,\ldots,MK$ such that the Lagrangian markers are denoted by $\mathbf{X} = \mathbf{X}(s_k) = (R_k, Z_k)$. The surfactant concentration Γ_k and surface tension σ_k are defined at the half-integer points given by $s_{k-1/2} = (k-1/2)\Delta s$. Without loss of generality, for any function defined on the interface $\phi(s)$, we approximate the partial derivative $\partial\phi/\partial s$ by

$$D_s\phi(s) = \frac{\phi(s+\Delta s/2) - \phi(s-\Delta s/2)}{\Delta s}. \tag{3.1}$$

Since $|D_s\mathbf{X}_k|$ can approximate the interface stretching factor by using this finite difference convention, the unit tangent vector $\boldsymbol{\tau}_k$ are defined at the half-integer points.

Let Δt be the time step size, and n be the superscript time step index. At the beginning of each time step, e.g., step n, the variables $\mathbf{X}_k^n = \mathbf{X}(s_k, n\Delta t), \Gamma_k^n = \Gamma\left(s_{k-1/2}, n\Delta t\right), \mathbf{u}^n = \mathbf{u}(\mathbf{x}, n\Delta t)$, and $p^n = p(\mathbf{x}, n\Delta t)$ are all given. The details of the numerical time integration are as follows.

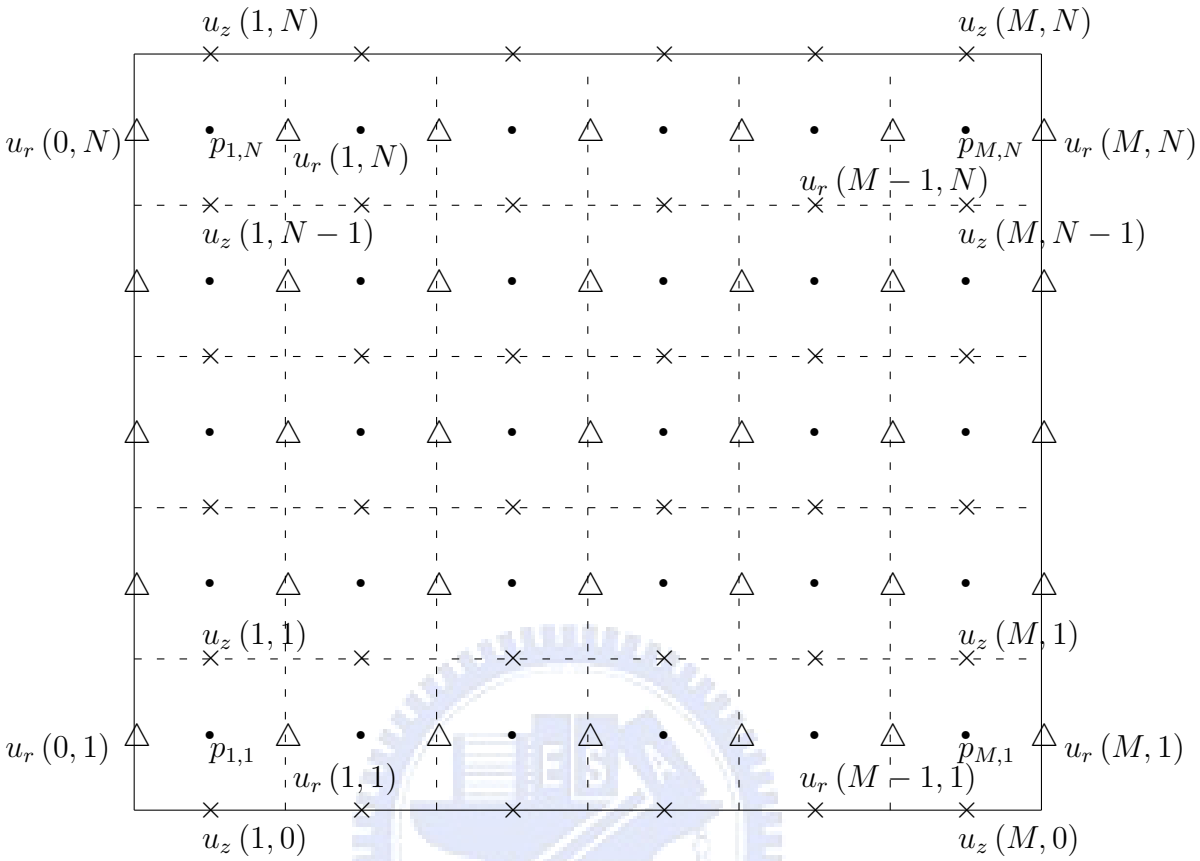

Figure 3.1: The computational domain Ω using staggered grid with mesh size h.

1. Surface tension and unit tangent vector
   Compute the surface tension and unit tangent vector on the interface as

$$\sigma_k^n = \sigma_c\left(1-\beta\Gamma_k^n\right), \tag{3.2}$$

$$\boldsymbol{\tau}_k^n = \frac{D_s\mathbf{X}_k^n}{|D_s\mathbf{X}_k^n|}, \tag{3.3}$$

   both of which hold for $s_{k-1/2} = (k-1/2)\Delta s$. Then we define the interfacial force as

$$\mathbf{F}_k^n = D_s\left(\sigma_k^n\boldsymbol{\tau}_k^n\right) - \frac{D_sZ_k^n}{R_k^n}\left(\boldsymbol{\tau}_k^n\mathbf{n}_k^n\right), \tag{3.4}$$

   at point $\mathbf{X}_k$.

2. Force to the fluid
   Distribute the force from the markers to the fluid by

$$\mathbf{f}^n\left(\mathbf{x}\right) = \sum_k \mathbf{F}_k^n\delta_h\left(\mathbf{x}-\mathbf{X}_k^n\right)\Delta s, \tag{3.5}$$

where the smooth version of Dirac delta function,

$$\delta_h(x) = \begin{cases} \frac{1}{4h}\left(1+\cos\left(\frac{\pi x}{2h}\right)\right), & \text{if } -2h \le x \le 2h \\ 0, & \text{otherwise,} \end{cases} \tag{3.6}$$

is used.

3. Navier-Stokes equations
Solve the Navier-Stokes equations. This can be done by the following semi-implicit second-order projection scheme, where the nonlinear term is approximated by a second-order extrapolation to avoid solving a nonlinear system at each time step.

$$\begin{aligned}
&\rho^n \left[\frac{3\tilde{u_r}^{n+1} - 4u_r^n + u_r^{n-1}}{2\Delta t} + \left(2u_r^n\frac{\partial u_r^n}{\partial r} - u_r^{n-1}\frac{\partial u_r^{n-1}}{\partial r}\right) + \left(2u_z^n\frac{\partial u_r^n}{\partial z} - u_z^{n-1}\frac{\partial u_r^{n-1}}{\partial z}\right)\right] \\
&= -\frac{\partial p^n}{\partial r} + \frac{1}{Re}\{\frac{2}{r}\frac{\partial}{\partial r}\left(r\mu^n\frac{\partial \tilde{u_r}^{n+1}}{\partial r}\right) + \frac{\partial}{\partial z}\left(\mu^n\frac{\partial u_z^n}{\partial r}\right) + \frac{\partial}{\partial z}\left(\mu^n\frac{\partial u_r^n}{\partial r}\right) - \frac{2\mu^n\tilde{u_r}^{n+1}}{r^2}\} \\
&\quad + \frac{1}{ReCa}f_r^n \\
&\rho^n \left[\frac{3\tilde{u_z}^{n+1} - 4u_z^n + u_z^{n-1}}{2\Delta t} + \left(2u_r^n\frac{\partial u_z^n}{\partial r} - u_r^{n-1}\frac{\partial u_z^{n-1}}{\partial r}\right) + \left(2u_z^n\frac{\partial u_z^n}{\partial z} - u_z^{n-1}\frac{\partial u_z^{n-1}}{\partial z}\right)\right] \\
&= -\frac{\partial p^n}{\partial z} + \frac{1}{Re}\{\frac{1}{r}\frac{\partial}{\partial r}\left(r\mu^n\frac{\partial \tilde{u_z}^{n+1}}{\partial r}\right) + \frac{1}{r}\frac{\partial}{\partial r}\left(r\mu^n\frac{\partial u_r^n}{\partial z}\right) + 2\frac{\partial}{\partial z}\left(\mu^n\frac{\partial u_z^n}{\partial z}\right)\} \\
&\quad + \frac{1}{ReCa}f_z^n
\end{aligned} \tag{3.7}$$

$$\tilde{\mathbf{u}} = \mathbf{u}_b, \ on\, \partial\Omega, \tag{3.8}$$

$$\tilde{\nabla}_h \cdot \mathbf{u}^{n+1} = 0, \tag{3.9}$$

$$\tilde{\nabla}_h \cdot \left(\frac{1}{\rho^n}\tilde{\nabla}_h\phi^{n+1}\right) = \frac{3\tilde{\nabla}_h\cdot\tilde{\mathbf{u}}}{2\Delta t}, \ \frac{\partial\phi}{\partial\mathbf{n}} = 0, \ on\, \partial\Omega \tag{3.10}$$

$$\tilde{\nabla}_h\phi^{n+1} = \frac{3\rho^n\left(\tilde{\mathbf{u}}^{n+1} - \mathbf{u}^{n+1}\right)}{2\Delta t}, \tag{3.11}$$

$$p^{n+1} = p^n + \phi^{n+1}. \tag{3.12}$$

Here the gradient operator $\tilde{\nabla}_h = (\partial/\partial r, \partial/\partial z)$, the divergent operator $\tilde{\nabla}_h\cdot = (\frac{1}{r}\frac{\partial}{\partial r}r, \frac{\partial}{\partial z})\cdot$ and the Laplace operator

$$\tilde{\Delta}_h\tilde{\mathbf{u}}^{n+1} = \left(\frac{\partial^2 u_r^{n+1}}{\partial r^2} + \frac{1}{r}\frac{\partial u_r^{n+1}}{\partial r} + \frac{\partial^2 u_r^{n+1}}{\partial z^2} - \frac{u_r^{n+1}}{r^2}\ ,\ \frac{\partial^2 u_z^{n+1}}{\partial r^2} + \frac{1}{r}\frac{\partial u_z^{n+1}}{\partial r} + \frac{\partial^2 u_z^{n+1}}{\partial z^2}\right)$$

$$\tilde{\nabla}_h^2 \phi^{n+1} = \frac{\partial^2 \phi^{n+1}}{\partial r^2} + \frac{1}{r}\frac{\partial \phi^{n+1}}{\partial r} + \frac{\partial^2 \phi^{n+1}}{\partial z^2}$$

are the standard centered difference operator on the grid which is defined at the staggered grid mesh. One can see that the above Navier-Stokes solver involves solving two Helmholtz equations for velocity $\tilde{\mathbf{u}}^{n+1}$ and one Poisson equation for pressure. These elliptic equations are solved by using the direct sparse solver which is provided by CXML.

4. Ghost values form boundary condition
   The numercial experiment in next section is concerned with a drop in a extensional flow. In this case, the initial condition of a extensional flow $\mathbf{u} = G(-0.5r, z)$ is applied in the beginning. The velocity of the computational domain is $[a, b] \times [c, d]$ where $a = 0$ because of axisymmetric, and the boundary conditions of the velocities are $u_r = 0$ and $\partial u_z/\partial r = 0$ on $r = 0$. That is,$u_r(r, c) = -0.5rG, u_r(r, d) = -0.5rG, u_r(a, z) = 0, u_r(b, z) = -0.5bG$,and $u_z(r, c) = cG, u_z(r, d) = dG, u_z(a, z) = zG, u_z(b, z) = zG$. Then approximations for ghost values from linear extrapolation are given in the following.

$$\begin{aligned}
u_r(i, 0) &= -rG - u_r(i, 1), \\
u_r(i, N+1) &= -rG - u_r(i, N), \\
u_r(0, j) &= 0, \\
u_r(M, j) &= -0.5bG; \\
u_z(i, 0) &= cG, \\
u_z(i, N) &= dG, \\
u_z(0, j) &= -u_z(1, j), \\
u_z(M+1, j) &= 2zG - u_z(M, j).
\end{aligned}$$

   Note that $u_r(i, 1), u_r(i, N), u_z(1, j), and u_z(M+1, j)$ are unknowns for the system when these ghost values are used. Therefore, the effect of these ghost values will appear in the right-hand side of the linear system and simultaneously affect the coefficients of the linear system.

5. Updating position of marks
   Interpolate the new velocity on the fluid lattice points onto the marker points and move the marker points to new positions.

$$\mathbf{U}_k^{n+1} = \sum_{\mathbf{x}} \mathbf{u}^{n+1} \delta_h(\mathbf{x} - \mathbf{X}_k^n) h^2, \tag{3.13}$$

$$\mathbf{X}_k^{n+1} = \mathbf{X}_k^n + \Delta t \mathbf{U}_k^{n+1}. \tag{3.14}$$

In order to redistribute the interfacial markers more uniformly, we should add the artificial velocity,

$$U^{A}{}_{k}^{n+1} = \frac{k\Delta s}{2\pi}\sum_{k'=0}^{M} D_s\mathbf{U}_k^{n+1}\cdot\boldsymbol{\tau}_k^{n+1}\Delta s - \sum_{k'=0}^{k} D_s\mathbf{U}_k^{n+1}\cdot\boldsymbol{\tau}_k^{n+1}\Delta s. \tag{3.15}$$

From the above equations, we have the modified marker positions,

$$\mathbf{X}_k^{n+1} = \mathbf{X}_k^n + \Delta t\mathbf{U}_k^{n+1} + \Delta t U^{A}{}_{k}^{n+1}\boldsymbol{\tau}_k^{n+1}. \tag{3.16}$$

6. Update surfactant concentration distributionΓ_k^{n+1}
Since the surfactant is insoluble, the total mass on the interface must be conserved. Thus, it is important to develop a numerical scheme for the surfactant concentration equation to preserve the total mass. This can be done as follows. Substitute Eq.(2.27) of rate of stretching factor into the Eq.(2.29), we have

$$R\left|\frac{\partial\mathbf{X}}{\partial s}\right|\frac{\partial\Gamma}{\partial t} + \frac{\partial}{\partial t}\left(\left|\frac{\partial\mathbf{X}}{\partial s}\right|R\right)\Gamma = \frac{1}{Pe_s}\frac{\partial}{\partial s}\left[\left(R\frac{\partial\Gamma}{\partial s}\right)\Big/\left|\frac{\partial\mathbf{X}}{\partial s}\right|\right] \tag{3.17}$$

Now we discretiz the above equation by the Crank-Nicholson scheme in a symmetric way as

$$\begin{aligned}
&\frac{\Gamma_k^{n+1}-\Gamma_k^n}{\Delta t}\frac{r_k^{n+1}\left|D_s\mathbf{X}_k^{n+1}\right| + R_k^n\left|D_s\mathbf{X}_k^n\right|}{2} + \frac{R_k^{n+1}\left|D_s\mathbf{X}_k^{n+1}\right| - R_k^n\left|D_s\mathbf{X}_k^n\right|}{\Delta t}\frac{\Gamma_k^{n+1}+\Gamma_k^n}{2} \\
&= \frac{1}{Pe_s}\frac{1}{\Delta s}\left[\frac{R_{k+1/2}^{n+1}}{|D_s\mathbf{X}_{k+1}^{n+1}| + |D_s\mathbf{X}_k^{n+1}|}\frac{\Gamma_{k+1}^{n+1}-\Gamma_k^{n+1}}{\Delta s} - \frac{R_{k-1/2}^{n+1}}{|D_s\mathbf{X}_k^{n+1}| + |D_s\mathbf{X}_{k-1}^{n+1}|}\frac{\Gamma_k^{n+1}-\Gamma_{k-1}^{n+1}}{\Delta s}\right. \\
&\qquad\left. + \frac{R_{k+1/2}^{n}}{\left|D_s\mathbf{X}_{k+1}^{n}\right| + |D_s\mathbf{X}_k^{n}|}\frac{\Gamma_{k+1}^{n}-\Gamma_k^{n}}{\Delta s} - \frac{R_{k-1/2}^{n}}{|D_s\mathbf{X}_k^{n}| + \left|D_s\mathbf{X}_{k-1}^{n}\right|}\frac{\Gamma_k^{n}-\Gamma_{k-1}^{n}}{\Delta s}\right]
\end{aligned} \tag{3.18}$$

Where k is "half-integer" index, i.e. $k = 0.5, 1.5, \ldots, MK - 1/2$. According to the new interfacial marker position $\mathbf{X}_k^{n+1}$ obtained in the previous step and the boundary condition $(\Gamma_k^{n+1} - \Gamma_{k-1}^{n+1})/\Delta s = 0$, where $k = 0.5$ or $MK + 1/2$, on the endpoints of the interface, Eq.(3.18) results in a symmetric tri-diagonal linear system which can be solved easily. More importantly, the total mass of surfactant is conserved numerically; that is,

$$\sum_k \Gamma_k^{n+1}|D_s\mathbf{X}_k^{n+1}|R_{k-1/2}^{n+1}\Delta s = \sum_k \Gamma_k^n|D_s\mathbf{X}_k^n|R_{k-1/2}^n\Delta s \tag{3.19}$$

The summation in Eq.(3.19) is the mid-point rule discretization for the integral in Eq.(2.25).The thing that the total mass is conserved can be derived

by taking the summation of both sides of Eq.(3.18) and using the boundary condition.

Note that, when the artificial velocity is imposed on our equations like Eq.(3.16), Eq.(3.18) also have to impose the artificial velocity as follows.

$$\begin{aligned}
&\frac{\Gamma_k^{n+1}-\Gamma_k^n}{\Delta t}\frac{R_k^{n+1}\left|D_s\mathbf{X}_k^{n+1}\right|+R_k^n\left|D_s\mathbf{X}_k^n\right|}{2}+\frac{R_k^{n+1}\left|D_s\mathbf{X}_k^{n+1}\right|-R_k^n\left|D_s\mathbf{X}_k^n\right|}{\Delta t}\frac{\Gamma_k^{n+1}+\Gamma_k^n}{2}\\
&\quad-\left[\frac{R_{k+1/2}^{n+1}U^{A}{}_{k+1/2}^{n+1}\left(\Gamma_{k+1}^{n+1}+\Gamma_k^{n+1}\right)/2-r_{k-1/2}^{n+1}U^{A}{}_{k-1/2}^{n+1}\left(\Gamma_k^{n+1}+\Gamma_{k-1}^{n+1}\right)/2}{2\Delta s}\right.\\
&\quad\left.+\frac{R_{k+1/2}^{n}U^{A}{}_{k+1/2}^{n}\left(\Gamma_{k+1}^{n}+\Gamma_k^{n}\right)/2-R_{k-1/2}^{n}U^{A}{}_{k-1/2}^{n}\left(\Gamma_k^{n}+\Gamma_{k-1}^{n}\right)/2}{2\Delta s}\right]\\
&=\frac{1}{Pe_s}\frac{1}{\Delta s}\left[\frac{R_{k+1/2}^{n+1}}{|D_s\mathbf{X}_{k+1}^{n+1}|+|D_s\mathbf{X}_k^{n+1}|}\frac{\Gamma_{k+1}^{n+1}-\Gamma_k^{n+1}}{\Delta s}-\frac{R_{k-1/2}^{n+1}}{|D_s\mathbf{X}_k^{n+1}|+|D_s\mathbf{X}_{k-1}^{n+1}|}\frac{\Gamma_k^{n+1}-\Gamma_{k-1}^{n+1}}{\Delta s}\right.\\
&\quad\left.+\frac{R_{k+1/2}^{n}}{\left|D_s\mathbf{X}_{k+1}^{n}\right|+|D_s\mathbf{X}_k^{n}|}\frac{\Gamma_{k+1}^{n}-\Gamma_k^{n}}{\Delta s}-\frac{R_{k-1/2}^{n}}{|D_s\mathbf{X}_k^{n}|+\left|D_s\mathbf{X}_{k-1}^{n}\right|}\frac{\Gamma_k^{n}-\Gamma_{k-1}^{n}}{\Delta s}\right] \qquad (3.20)
\end{aligned}$$

7. Update density and viscosity
   Since the density and viscosity are discontinuous constants across the interface, they can be represented by Eq.(2.34)and Eg.(2.35). By Eq.(2.32) and Lapace operator in the cylindrical coordinates, we obtain

$$\begin{aligned}
\tilde{\Delta}_h I_{i,j} &= \frac{I_{i+1,j}-2I_{i,j}+I_{i-1,j}}{\Delta r^2}+\frac{1}{r_i}\frac{I_{i+1,j}-I_{i-1,j}}{2\Delta r}+\frac{I_{i,j+1}-2I_{i,j}+I_{i,j-1}}{\Delta z^2},\\
&\qquad\qquad \frac{\partial I}{\partial \mathbf{n}}=0,\ \ on\,\partial\Omega\\
&= \frac{G_{i+1/2,j}-G_{i-1/2,j}}{\Delta r}+\frac{G_{i,j}}{r_i}+\frac{G_{i,j+1/2}-G_{i-1,j-1/2}}{\Delta z} \qquad (3.21)
\end{aligned}$$

where,

$$\mathbf{G}_{i,j}=\begin{pmatrix} G_{i+1/2,j}\\ G_{i,j+1/2}\end{pmatrix}=\begin{pmatrix} \sum\limits_k n_k^1 d_h\left(r_{i+1/2,j}-R_k\right)d_h\left(z_{i,j}-Z_k\right)d_h\Delta s\\ \sum\limits_k n_k^2 d_h\left(r_{i,j}-R_k\right)d_h\left(z_{i,j+1/2}-Z_k\right)d_h\Delta s\end{pmatrix}$$

4 Numerical results

4.1 convergent test

First of all, we test the convergence of Navier-Stokes solver. Here, we perform different computations with varying meshes $h = \Delta r = \Delta z = 1/32, 1/64, 1/128$,and the time step size is $\Delta t = h/4$.The solutions are computed up to time $T = 1$.The problem is set up in fluid domain $\Omega = [0, 1] \times [-1, 1]$, the Reynolds number $R_e = 1$ and the capillary number $Ca = 1$. We set exact solutions as follows and f_r, f_z obtain by E.q.(2.15) ,E.q.(2.16).

$$\begin{aligned} u_r(r,z,t) &= \frac{\pi}{2} r^3 cos(\pi z) e^{-t} \\ u_z(r,z,t) &= r^2 (cos(\pi r) - 2sin(\pi z)) e^{-t} \\ p(r,z,t) &= cos(2\pi r) cos(\pi z) e^{-t} \end{aligned}$$

When,

$$\begin{aligned} \rho(r,z,t) &= 1 \\ \mu(r,z,t) &= 1 \end{aligned}$$

Table 1: The mesh refinement analysis of the velocity u_r, u_z.

h	$\|u_r - u_{exact}\|_\infty$	Rate	$\|u_z - u_{exact}\|_\infty$	Rate
1/32	$4.6868E-04$	-	$7.7483E-04$	-
1/64	$2.0812E-04$	1.1712	$4.1138E-04$	0.9134
1/128	$1.1699E-04$	0.8310	$2.2038E-04$	0.9005

When,

$$\begin{aligned} \rho(r,z,t) &= (1.5 + cos(\pi r)) e^{-t} \\ \mu(r,z,t) &= 1 \end{aligned}$$

Table 2: The mesh refinement analysis of the velocity u_r, u_z.

h	$\|u_r - u_{exact}\|_\infty$	Rate	$\|u_z - u_{exact}\|_\infty$	Rate
1/32	$6.1872E-04$	-	$7.6975E-04$	-
1/64	$2.1793E-04$	1.5054	$4.2531E-04$	0.8559
1/128	$1.1867E-04$	0.8769	$2.2278E-04$	0.9329

When,

$$\begin{aligned}\rho(r,z,t) &= (1.5+cos(\pi r))\,e^{-t}\\ \mu(r,z,t) &= \left(\left(2r^3-3r^2\right)cos(\pi z)+1\right)e^{-t}\end{aligned}$$

Table 3: The mesh refinement analysis of the velocity u_r, u_z.

h	$\|u_r - u_{exact}\|_\infty$	Rate	$\|u_z - u_{exact}\|_\infty$	Rate
1/32	$6.3648E-04$	-	$8.9644E-04$	-
1/64	$2.3356E-04$	1.4463	$5.4650E-04$	0.7140
1/128	$1.2293E-04$	0.9260	$3.3458E-04$	0.7079

Table 3 shows the mesh refinement analysis of the velocity u_r, u_z. One can see that the error decreases substantially when the mesh is refined, and the rate of convergence is somewhat first order. Note that, the fluid variables are defined at the staggered grid in $r-z$ coordinates, but the density and viscosity are defined at the center of of the uniform grid. In addition there are some cross derivative terms in our equations, so it is not fully implicit. Thus it is why the rate of convergence behaves less than second-order.

After above test, we impose the surfactant on the interface to observe the drop behavior. We observe effects of the clean drop deformation on the viscosity in an extensional flow , $u_r = -0.5Gr$ and $u_z = Gz$, where G is the principal strain rate [6], and is chosen as $G = 1$. The computational domain is chosen as $\Omega = [0,1]\times[-1,1]$ in the axisymmetrical cylindrical coordinates, and the initial drop is chosen as a circular one with radius $r_0 = 0.25$. We choose $\beta = 1$ for the surface tension equation Eq.2.2.3. In order to make our research convinced, we should carry out the convergence study of the immersed boundary method. We use the different mesh $h = \Delta r = \Delta z = 1/32, 1/64, 1/128$ and $1/256$ to perform our computation relatively. The Lagrangian mesh is chosen as $\Delta s \approx h$ and the time step size is $\Delta t = h/8$. The solutions are computed up to time T = 1. Since it is not easy to obtain the analytical solution from our problem, we choose the finest mesh as our reference solution to compute the L_∞ error between the reference solution and the solution which is solved from the coarser grid. Here, we choose Reynolds number $Re = 1$, Capillary number $Ca = 0.25$, Peclet number $Pes = 12.5$, the viscosity inside drop $\mu_1 = 5$, and the viscosity outside drop $\mu_2 = 1$.

Table 4: The mesh refinement analysis of the velocity u_r, u_z, and the surfactant concentration Γ.

h	$\|u_r - U_{Rref}\|_\infty$	Rate	$\|u_z - U_{Zref}\|_\infty$	Rate	$\|\Gamma - \Gamma_{ref}\|_\infty$	Rate
1/32	$7.2843E-03$	-	$8.4765E-03$	-	$1.1299E-02$	-
1/64	$3.9920E-03$	0.8677	$3.7282E-03$	1.1850	$6.2283E-03$	0.8593
1/128	$2.0879E-03$	0.9350	$1.3146E-03$	1.4744	$2.4108E-03$	1.3692

Table 4 shows that the error of $\|u_r - U_{Rref}\|_\infty$, $\|u_z - U_{Zref}\|_\infty$, and $\|\Gamma - \Gamma_{ref}\|_\infty$ converge to zero where U_{Rref}, U_{Zref}, and Γ_{ref} are r-axial, z-axial reference velocities, and reference surfactant concentration relatively. The convergent rates for u_r, u_z, and Γ are about first order, but our method is a second order scheme. Note that since the fluid velocities are defined at the staggered grid in $r-z$ coordinates, the refined mesh will not coincide with the same grid locations. Thus, we approximate the coarser grid by cubic spline interpolation the velocities obtained from the reference grid near the coarser grid. In addition there are some cross derivative terms in our equations, so it is not fully implicit. We attribute this is part of the reason why the rate of convergence behaves less than second-order. Similarly, the surfactant concentration is defined at "half-integer" grid. When we average the reference grid, we should use the weighted average since the concentration is the mass per unit surface area.

4.2 Oscillating drop

Before to proceed, it is important to check how much the drop volume leaks or bulks up since it affects the computational accuracy. We test a simple case that a spheroid drop in the static liquid will be shrunk and turn into a sphere drop. This computational domain is set up as $\Omega = [0,1] \times [-1,1]$ in the axisymmetrical cylindrical coordinates, and put a spheroid drop with the semi-major axis whose length is $a = 3/4$ and with the semi-minor axis whose length is $b = 1/3$, respectively into our domain. Then, given the computational mesh $h = \Delta r = \Delta z$, $\Delta t = h/8$, the Reynolds number $Re = 25$, the Capillary number $Ca = 0.04$, and the surface Peclet number $Pe_s = 12.5$. The initial surfactant concentration is uniformly distributed along the interface such as $\Gamma(0,s) = 0.5$. The parameters in E.q.2.23 are chosen as $\sigma_c = 1$ and $\beta = 0.5$,respectively. In the meanwhile, we consider the density inside and outside of the drop are $\mu_1 = 2$ and $\mu_2 = 1$, respectively, and we computed the relative error of the drop volume V_{er} by

$$V_{er} = \frac{|V - V_i|}{V_i}$$

, where V_i = initial volume.

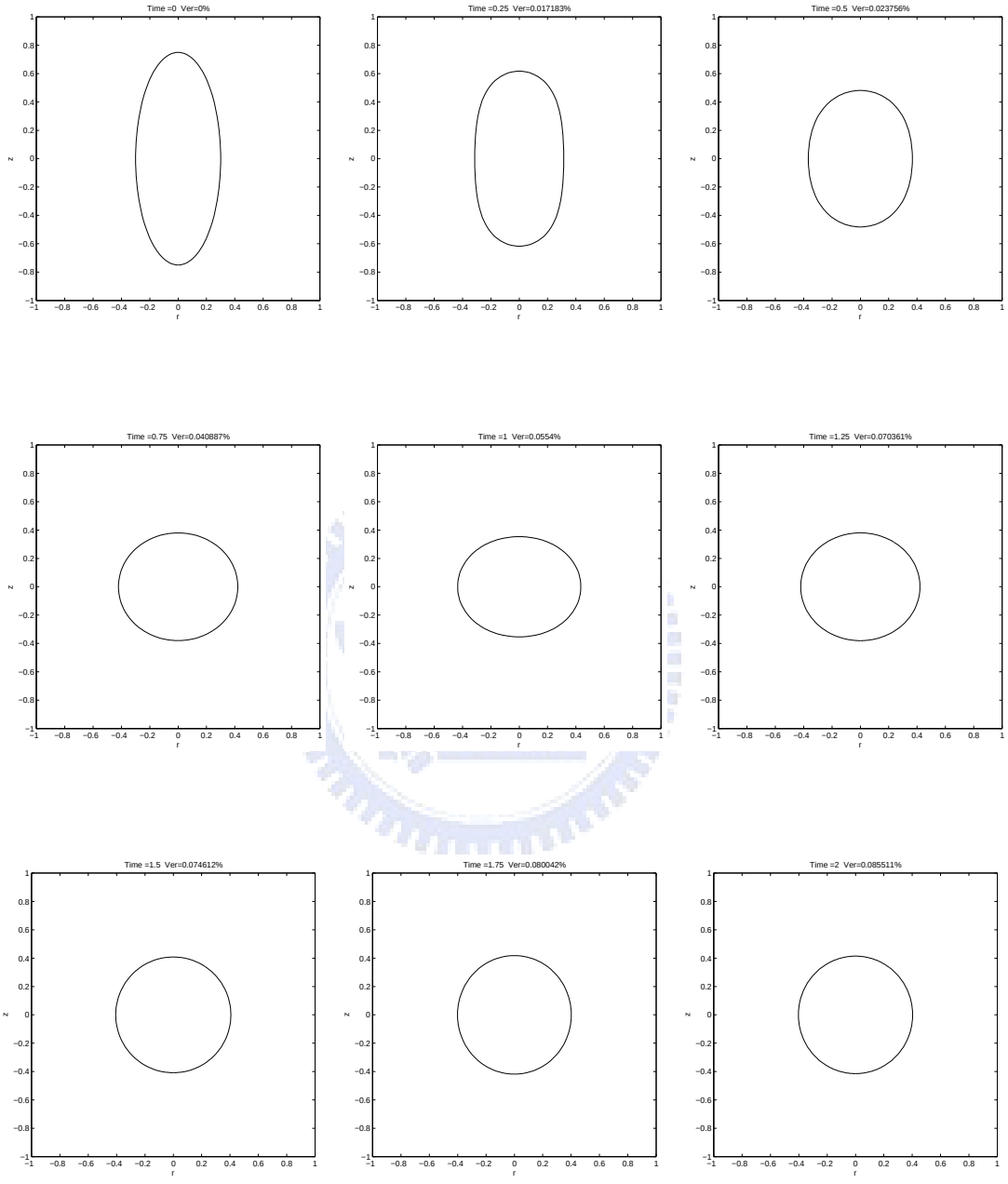

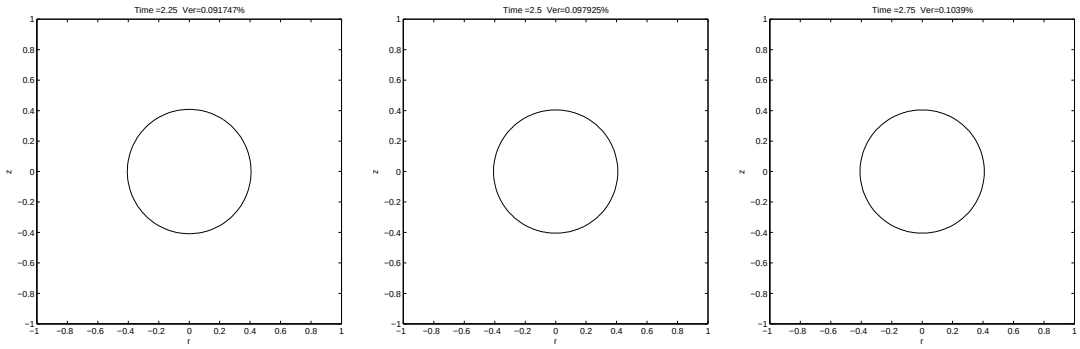

Figure 4.1: In the fluid velocity field, we observe the time evolution of a spheroid drop in a static liquid with $Re = 25$, $Ca = 0.04$ and $\Delta t = h/8$.

In figure 4.1, the oscillation of the drop depends on the fluid velocity field and the incompressibility of the drop. We also observe the distribution of the viscosity in figure 4.1. The spheroid drop with $a = 3/4$ and $b = 1/3$ oscillates from the time $T = 0$ to $T = 2$, and its steady state is the sphere drop with the radius $r \cong 0.4145$. After $T = 2$, the amplitude of vibration is smaller than the one before $T = 2$, but the drop volume leaks with the time evolution. The reason of this phenomenon is that there is the spurious velocities in our computational process. The spurious velocities influence the computation of the new marker positions on the interface .Thus, we only do our best to reduce the relative error of the drop volume. The relative error of the drop volume is smaller than 1% at $T = 2.75$ in figure 4.1. So, this is an acceptable error range for us.

4.3 Effects of the clean drop deformation on the viscosity

There is different viscosity inside the drop,so we will study it in this section. We observe effects of the clean drop deformation on the viscosity in an extensional flow , $u_r = -0.5Gr$ and $u_z = Gz$, where G is the principal strain rate [6], and is chosen as $G = 1$. Throughout this computation, the computational domain is chosen as $\Omega = [0, 1] \times [-3, 3]$ in the axisymmetrical cylindrical coordinates, and the initial drop is chosen as a circular one with radius $r_0 = 0.25$. We also fix the density inside and outside the drop $\rho_1 = \rho_2 = 1$, the Reynolds number $R_e = 1$, and the Capillary number $Ca = 0.6$. Here, we use the mesh $h = \Delta x = \Delta y = 1/64$, the Lagrangian grid with size $\Delta s \approx h$, the time step size $\Delta t = h/8$, and computed up to time $T = 4$. A convenient method for expressing the viscosity difference between two sides of drop is viscosity ratio λ, where μ_1 and μ_2 mean viscosity inside and outside the drop,

$$\lambda = \frac{\mu_1}{\mu_2}.$$

In general, a drop will be stretched along the direction of fluid flow if it is put into the extensional flow. But there is surface tension on the interface, it may restrict a tendency of stretching drop. Therefore,we first observe a property for the clean drop with the viscosity ratio $\lambda = 1, 5$ and 10, and we fix $\mu_2 = 1$ in this computation.

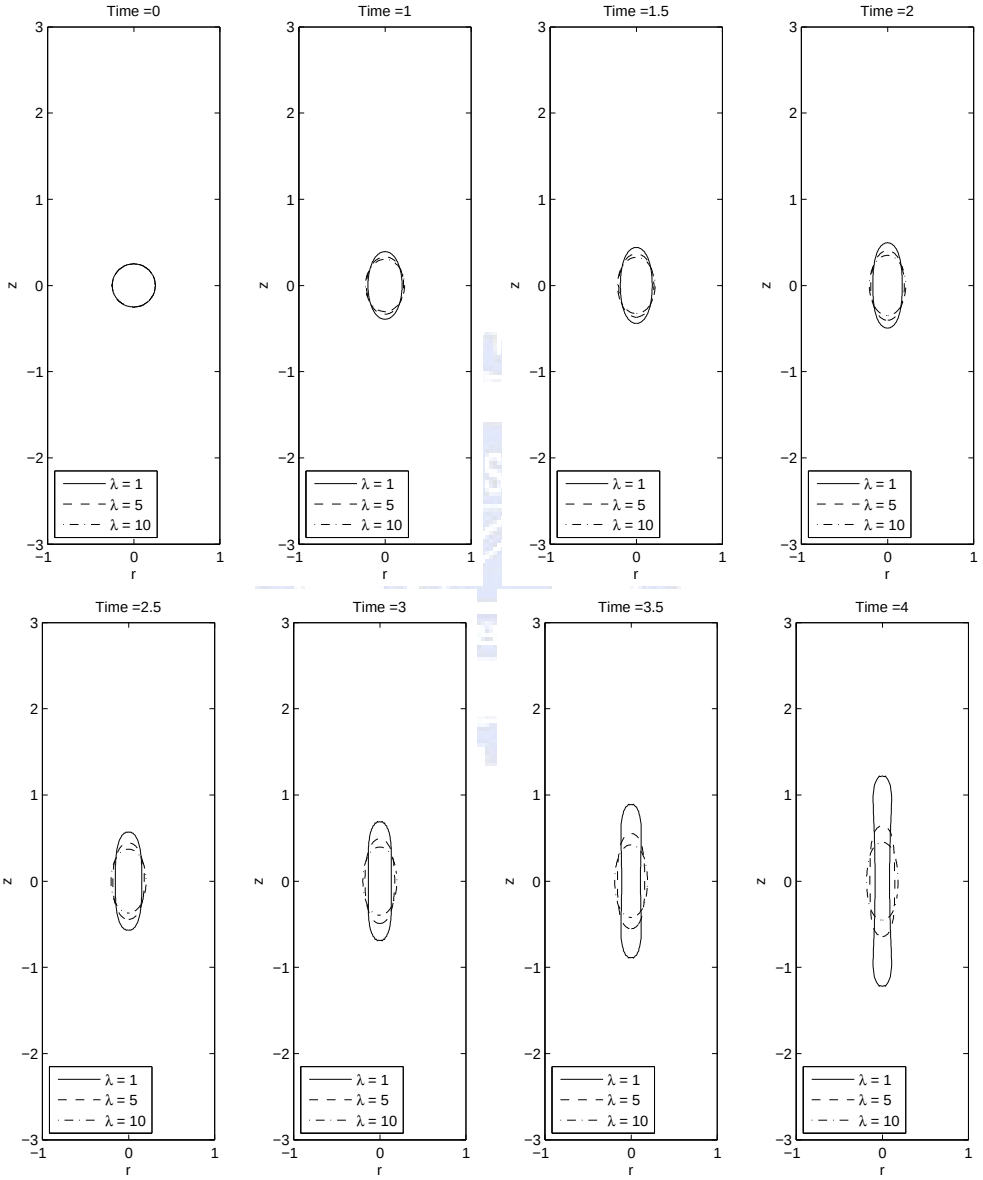

Figure 4.2: The time evolution of a drop in an extensional flow with $\lambda = 1, 5$ and 10 at $T = 4$.

Viscosity describes a fluid's internal resistance to flow and may be thought of as a measure of fluid friction. For example, high-viscosity magma will create a tall, steep stratovolcano, because it cannot flow far before it cools, while low-viscosity lava will create a wide, shallow-sloped shield volcano. We can observe the deformation of the drop by flow in Fig.4.2, and as $\lambda = 1, 5$, and 10 the tip point of the interface on the $z-$axis are at about the positions $(r, z) \approx (0, \pm 1.221), (0, \pm 0.6437)$ and $(0, \pm 0.4515)$,respectively at $T = 4$. By Eq.2.6 we know that E is the rate of deformation rate and the larger viscosity leads to smaller E. That is, the harde the drop will deform. We can observe this phenomenon from Fig.4.2. Thus drop is more sticky as viscosity is higher, the shape of drop is more difficult to be affected by flow.

We then examine how the bubble would deform when viscosity of the inside drop is smaller than that of outside drop, i.e., viscosity ratio $\lambda \leq 1$. We also observe effects of the clean drop deformation on the viscosity in an extensional flow , $u_r = -0.5Gr$ and $u_z = Gz$, where G is the principal strain rate [6], and is chosen as $G = 1$. Throughout this computation, the computational domain is chosen as $\Omega = [0, 1] \times [-3, 3]$ in the axisymmetrical cylindrical coordinates, and the initial drop is chosen as a circular one with radius $r_0 = 0.25$. We also fix the density inside and outside the drop $\rho_1 = \rho_2 = 1$, the viscosity inside drop $\mu_1 = 1$, the Reynolds number $R_e = 1$, and the Capillary number $Ca = 0.6$. Here, we use the mesh $h = \Delta x = \Delta y = 1/64$, the Lagrangian grid with size $\Delta s \approx h$, the time step size $\Delta t = h/8$, and computed up to time $T = 4$.

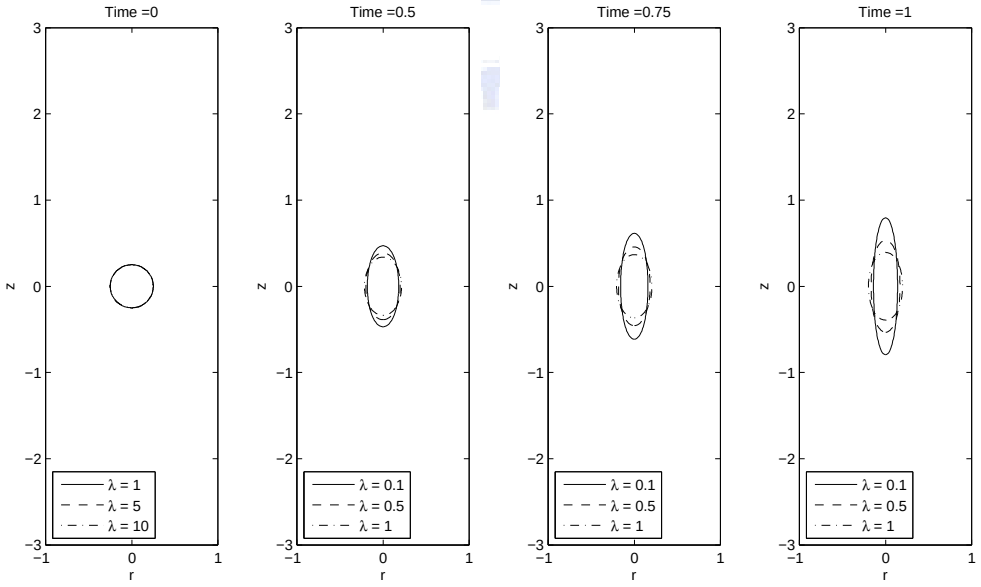

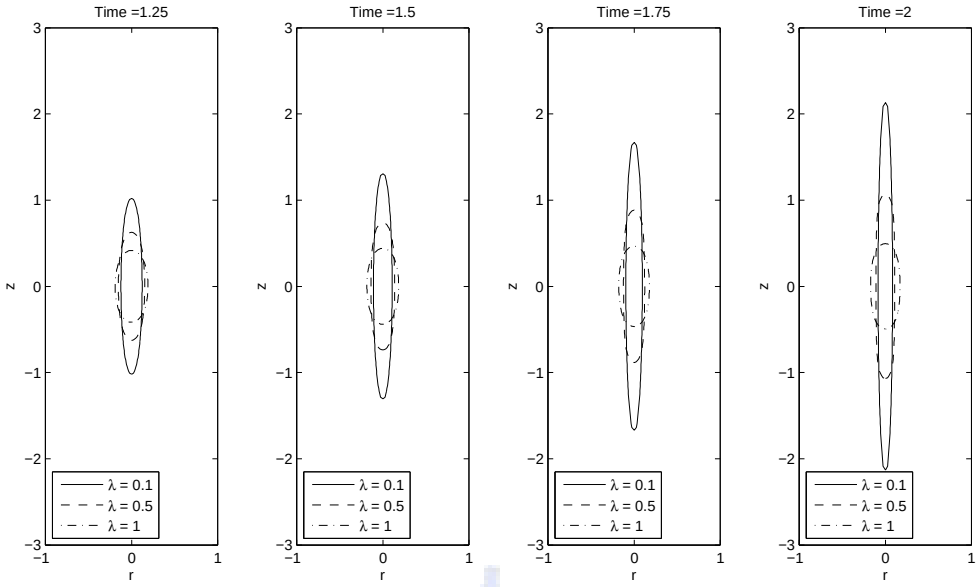

Figure 4.3: The time evolution of a drop in an extensional flow with $\lambda = 0.1, 0.5$ and 1 at $T = 2$.

We can observe the deformation of the drop by flow in Fig.4.3, and as $\lambda = 0.1, 0.5$, and 1 the tip point of the interface on the $z-$axis are at about the positions $(r, z) \approx (0, \pm 2.1323), (0, \pm 1.0702)$ and $(0, \pm 0.4951)$,respectively at $T = 2$. As above we observe the deformation of drop is more intense when viscosity ration is lower. From Fig.4.2 and Fig.4.3, we notice the velocity of drop deformation with viscosity ratio $\lambda < 1$ is faster than that with viscosity ratio $\lambda > 1$. By Eq.2.6 we know that E is the rate of deformation rate and the larger viscosity leads to smaller E. As viscosity ratio $\lambda < 1$, we can think of it as viscosity outside drop $\mu_2 < 1$ and viscosity inside drop $\mu_1 = 1$. Therefore we can perceive that the drop would be easier to deform from Fig.4.3. Thus drop is less sticky as viscosity is higher, the shape of drop is easier to be affected by flow.

4.4 Effects of the drop deformation on surfactant

There is different behavior for clean interface and contaminated interface, so we will study it in this subsection. We compare a clean drop with a contaminated drop in an extensional flow, $u_r = -0.5Gr$ and $u_z = Gz$, where $G = 1$. By the comparison, we observe that the surface tension reduces when the surfactant is on the interface. Here, we use the mesh $h = \Delta x = \Delta y = 1/64$, the Lagrangian grid with size $\Delta s \approx h$, and the time step size $\Delta t = h/8$.

The problem is set up as a drop immersed in a fluid domain $\Omega = [0, 1] \times [-3, 3]$ with viscosity 1, which the drop is a circle with radius $r_0 = 0.25$. We also fix the density inside and outside the drop $\rho_1 = \rho_2 = 1$, the Reynolds number $R_e = 1$, the Capillary number $Ca = 0.6$,and the surface Peclet number $P_{es} = 1.25$. The initial surfactant concentration is uniformly distributed along the interface such as $\Gamma(0, s) = 0.5$, and the parameters in E.q.2.23 are chosen as $\sigma_c = 1$ and $\beta = 0.5$,respectively. We examine viscosity ratio $\lambda = 1, 5$ and 10 repeatedly and observe the distinction between the clean interface (no surfactant) and contaminated interface (with surfactant).

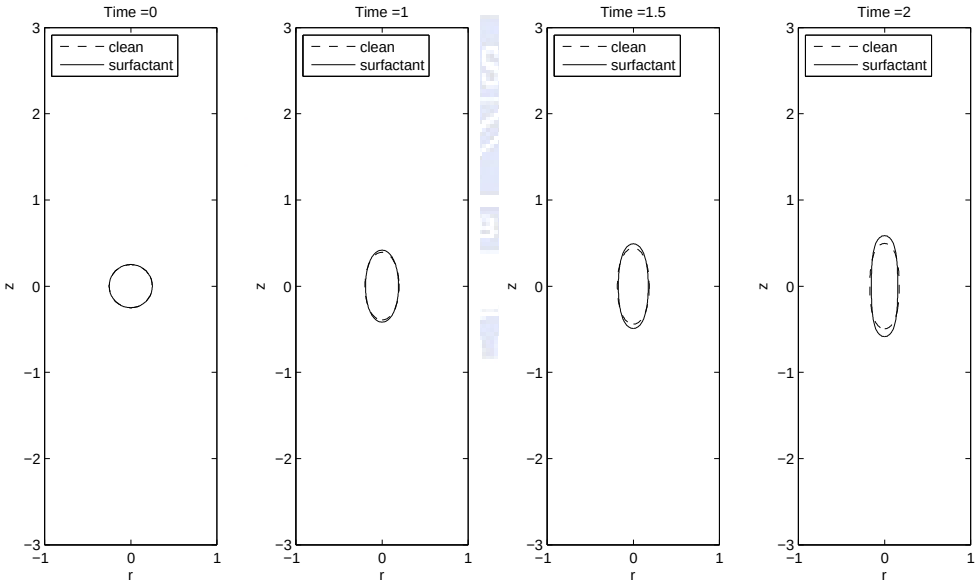

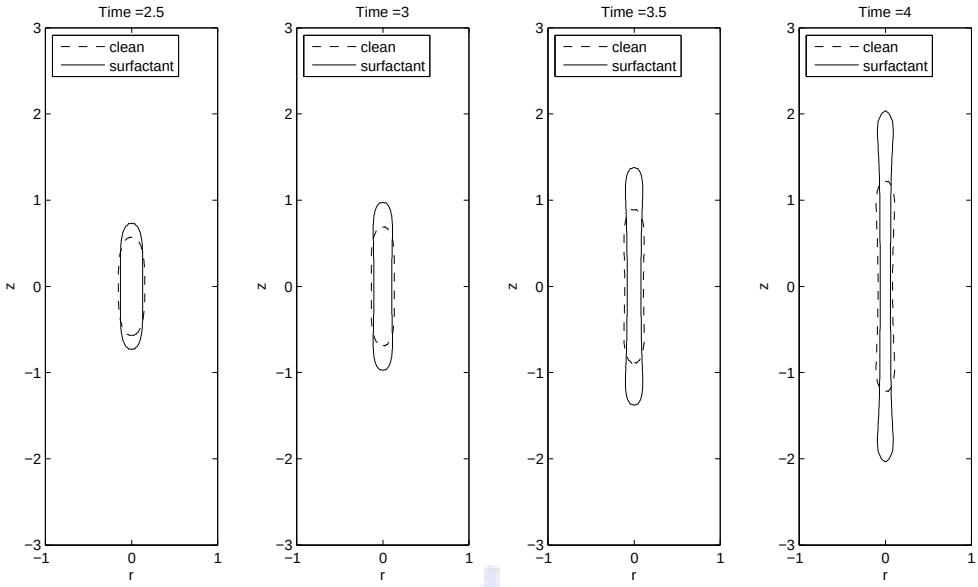

Figure 4.4: The time evolution of a drop in an extensional flow with $\lambda = 1$.

From the Fig4.4, the tip points of the interface on the z-axis are about at the positions $(r, z) \approx (0, \pm 2.0376)$, then we obtain the distance of contaminated drop from the tip point to the center is larger than that of clean drop. We observe the contaminated drop deforms more intensely because surfactant decrease the surface tension, causing the drop more likely to deform.

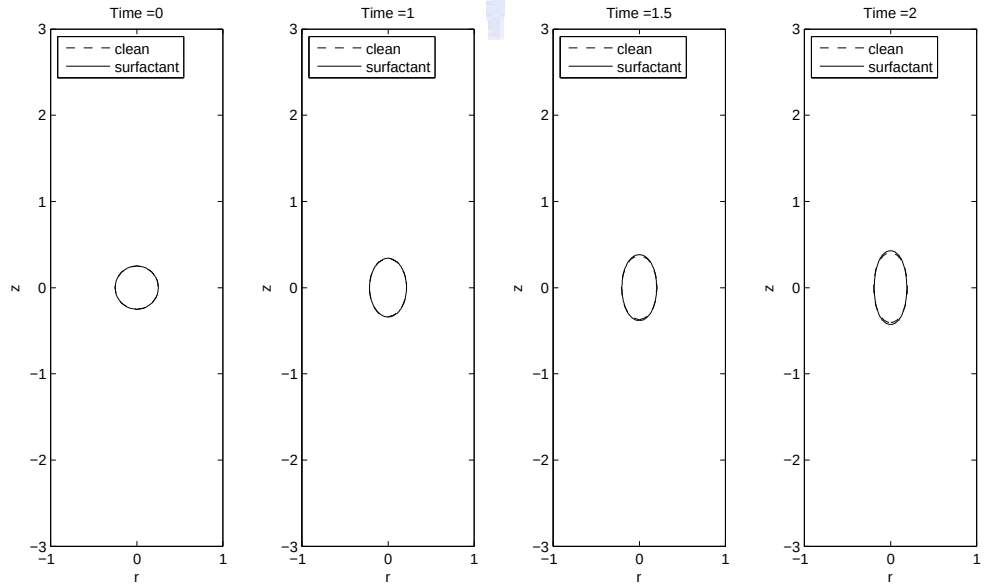

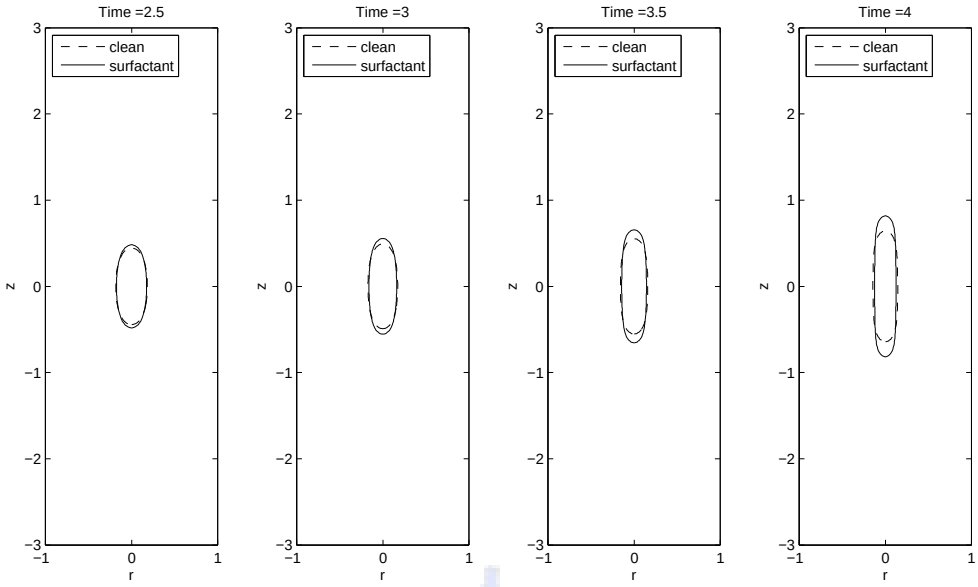

Figure 4.5: The time evolution of a drop in an extensional flow with $\lambda = 5$.

From the Fig4.5, the tip points of the interface on the z-axis are about at the positions $(r, z) \approx (0, \pm 0.8187)$, then we also obtain the distance of contaminated drop from the tip point to the center is larger than that of clean drop. Then, We examine viscosity ratio $\lambda = 10$ and observe the distinction between the clean interface (no surfactant) and contaminated interface (with surfactant).

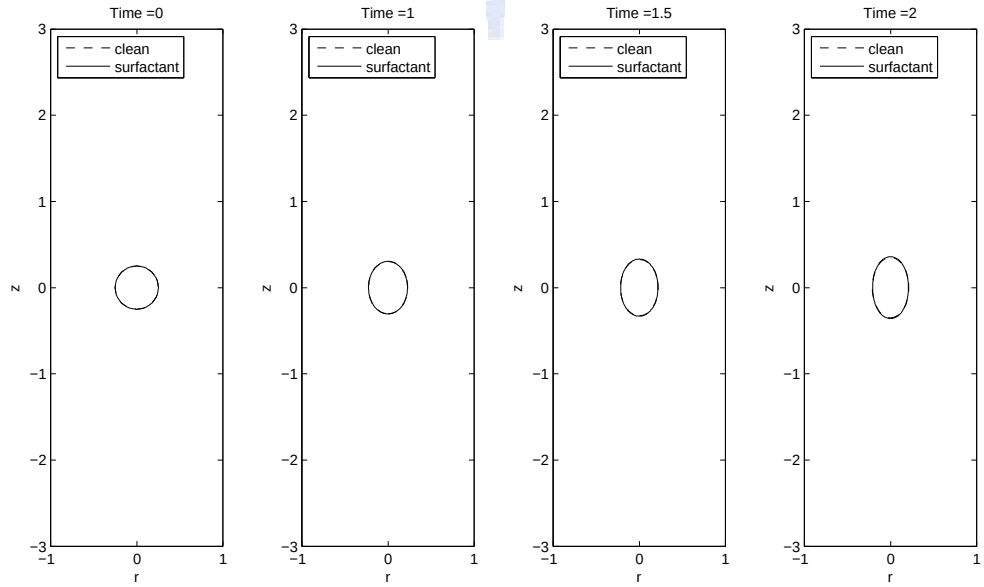

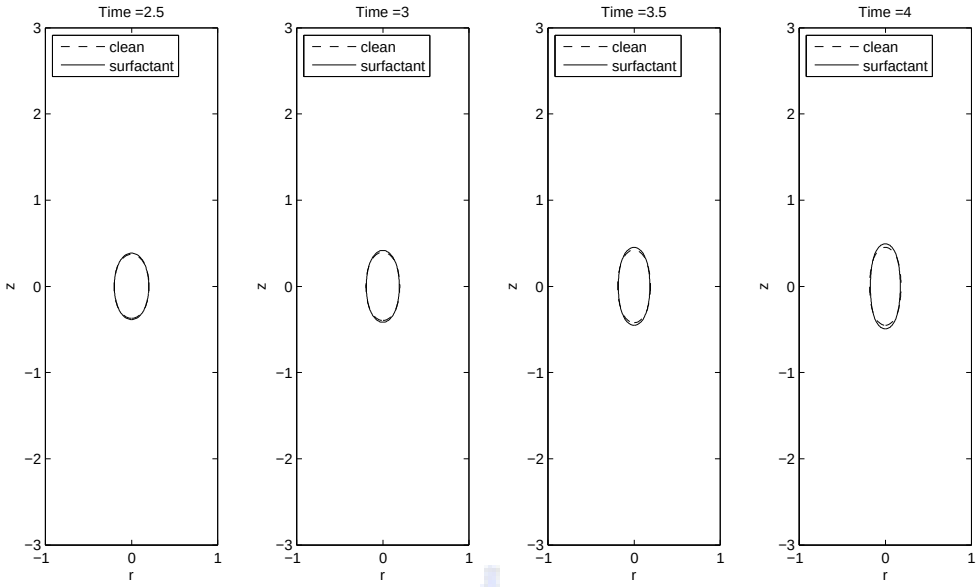

Figure 4.6: The time evolution of a drop in an extensional flow with $\lambda = 10$.

From the Fig4.6, the tip points of the interface on the z-axis are about at the positions $(r, z) \approx (0, \pm 0.4929)$, then we we also obtain the distance of contaminated drop from the tip point to the center is larger than that of clean drop.

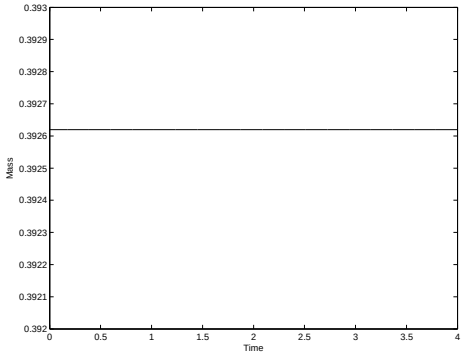

Figure 4.7: This is the total mass of surfactant for $Pe_s = 1.25$.

Even though surfactant would affect the drop deformation, viscosity is the main factor, and flow is more sticky as viscosity is higher, the shape of drop is more difficult to be affected by flow. Since the surfactant is insoluble, the total mass of the surfactant must be conserved In Fig.4.7, no matter which viscosity we choose, the total mass of surfactant for $Pe_s = 1.25$ is conserved very well by our method.

4.5 Effects of the drop deformation on Peclet number

In this subsection, we compare the influence of different surface Peclet number Pe_s on the elongation of contaminated drop, and we choose peclet number Pe_s from 0 to 500, partitioned 50 choices at once. Here, we first put a contaminated drop in the extensional flow, $u_r = -0.5Gr$ and $u_z = Gz$, where $G = 1$ and compute up to $T = 4$ in the domain $\Omega = [0, 1] \times [-3, 3]$. Then, we fix the Reynolds number $R_e = 1$, the Capillary number $Ca = 0.3$,and $\Gamma(0, s) = 0.5$ with the parameters in E.q.2.23 chosen as $\sigma_c = 1$ and $\beta = 0.5$,respectively.

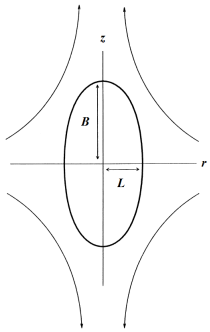

Figure 4.8: Drop in axisymmetric flow.

A convenient method for expressing the results of experiment is to measure L, the length of the drop in the direction of the r axis, and B, the breadth in the direction of the z axis. As noting in Fig.4.8, the degree of deformation can be characterized by the scalar D_f that was originally introduced by Taylor [11].

$$D_f = \frac{L - B}{L + B} \tag{4.1}$$

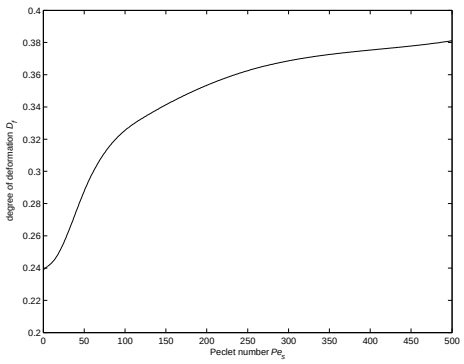

Figure 4.9: This is the deformation of drop with Peclet number Pe_s at $T = 4$.

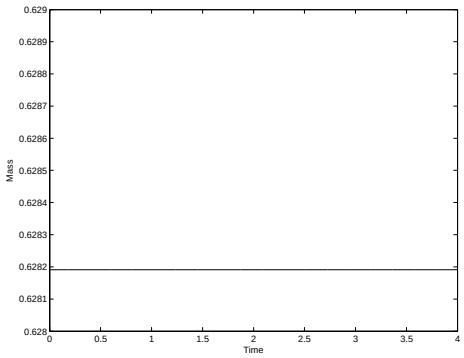

Figure 4.10: This is the total mass of surfactant for every Peclet number Pe_s.

Since the underlying extensional drives the surfactant toward to the tip points of the drop, the surfactant concentration is higher and thus the surface tension is lower near the tips. When the Peclet number is lager, the surfactant gradient along the interface is lager too, therefore, the overall drop elongation is greater. From Fig.4.9 we noticed from Peclet number Pe_s from 0 to 150 the larger the deformation the more obvious, but past 150 the larger the change will also be additional, but the higher the number the higher the tendency to plateau. By Fig.4.10 we also obtain the total mass of surfactant conserved no matter Peclet number which we choose.

5 Conclusion

In this paper, we used the immersed boundary method such that the interface is in the different phases with different densities and viscosities by an indicator function in the cylindrical coordinates to construct our formulation. Since the velocity field is in the axisymmetric coordinates, the velocity boundary conditions on $r = 0$ must be set $u_r = 0$ and $\partial u_z/\partial r = 0$.We solve the Navier-Stokes equations by projection method, and update the new marker positions by imposing the artificial velocity in order to make the new positions uniformly. Controlling marker positions uniformly can make the volume error smaller. Similarly, the surfactant equation must impose the artificial velocities to control the concentration locations. The surface tension is reduced by the surfactant, and Peclet number influences the diffusion of the surfactant.

In our future work, for a drop on a solid, controlling the equilibrium contact angle can produce the hydrophobic phenomenon or hydrophilic phenomenon. Imposing the surfactant on the interface affects the equilibrium contact angle in this moving contact line case. Furthermore, we can develop the more general 3-dimension simulation.

References

[1] David L. Brown, Ricardo Cortez, and Michael L. Minion, "Accurate projection methods for the incompressible NavierVStokes equations." *Journal of Computational Physics*, Vol. 168, (2001), pp. 464-499.

[2] Charles D. Eggleton, Tse-Min Tsai, and Kathleen J. Stebe, "Tip streaming from a drop in the presence of surfactants." *Physical Review Letters*, Vol. 87, No. 4, (2001), pp. from 048302-1 to 048302-4.

[3] Wei-Xi Huang, Soo Jai Shin, and Hyung Jin Sung, "Simulation of flexible filaments in a uniform flow by the immersed boundary method." *Journal of Computational Physics*, Vol. 226, (2007), pp. 2206-2228.

[4] Ming-Chih Lai, Wen-Wei Lin, and Weichung Wang, "A fast spectral/differnce method without pole conditions for Poisson-type equations in cylindrical and spherical geometries." *IMA Journal of Numerical Analysis*, Vol. 22, (2002), pp. 537-548.

[5] Ming-Chih Lai, Yu-Hau Tseng, and Huaxiong Huang, "An immersed boundary method for interfacial flows with insoluble surfactant." *Journal of Computational Physics*, Vol. 227, (2008), pp. 7279-7293.

[6] Jie Li, "The effect of an insoluble surfactant on the skin friction of a bubble." *European Journal of Mechanics B/Fluid*, 25 (2006) 59-73

[7] J. M. Lopez and Jie Shen, "An efficient spectral-projection method for the Navier-Stokes equations in cylindrical geometies, I. Axisymmetric cases." *Journal of Computational Physics*, Vol. 139, (1998), pp. 308-326.

[8] Charles S. Peskin and Beth Feller Printz, "Improved volume conservation in the computation of flows with immersed elastic boundaries." *Journal of Computational Physics*, Vol. 105, (1993), pp. 33-46.

[9] H.A. Stone, "A simple derivation of the time-dependent convective-diffusion equation for surfactant transport along adeforming interface." *Phys. Fluids* A 2 (1), (1990), pp. 111-112.

[10] H. A. Stone and L. G. Leal, "The effects of surfactants on drop deformation and breakup." *J. Fluid Mech.*, Vol. 220, (1990), pp. 161-186.

[11] G.I. Taylor, The formation of emulsions in definable fields of flow, Proc. R. Soc. Lond. A 146 (1934) 501.

[12] G. Tryggvason, B. Bunner, A. Esmaeeli, D. Juric, N. Al-Rawahi, W. Tauber, J. Han, S. Nas, Y.-J. Jan, A front-tracking method for the computations of multiphase flow, J. Comput. Phys., 169 (2001) 708-759

[13] Salih Ozen Unverdi and Grétar Tryggvason, "A Front-Tracking Method for Viscous, Incompressible, Multi-fluid Flows." *Journal of computational physics*, **100**, pp. 25-37 (1992)

[14] Etienne Guyon, Jean-Pierre Hulin, Luc Petit, and Catalin D. Mitescu,"Physical hydrodynamics." Oxford University Press, USA, (2001)